ACS Energy LETTERS

http://pubs.acs.org/journal/aelccp

LETTER

FACsPb Triple Halide Perovskite Solar Cells with Thermal Operation over 200 °C

Hadi Afshari,* Shashi Sourabh, Sergio A. Chacon, Vincent R. Whiteside, Rachel C. Penner, Bibhudutta Rout, Ahmad R. Kirmani, Joseph M. Luther, Giles E. Eperon, and Ian R. Sellers*

Cite This: *ACS Energy Lett.* 2023, 8, 2408−2413

Read Online

ACCESS | Metrics & More | Article Recommendations | Supporting Information

ABSTRACT: Formamidinium cesium (FACs) perovskites solar cells have been shown to be among the most stable metal halide perovskites. Here, high-temperature data are presented which systematically and statistically demonstrate the high thermal operation of this system to temperatures in excess of 200 °C. Device measurements between 250 K and 490 K show that while some loss of performance is evident at higher temperature, this is driven by reversible halide segregation with no evidence of a structural phase transition over the measurement range probed. Moreover, upon reduction of the temperature back to ambient the power conversion efficiency is retained.

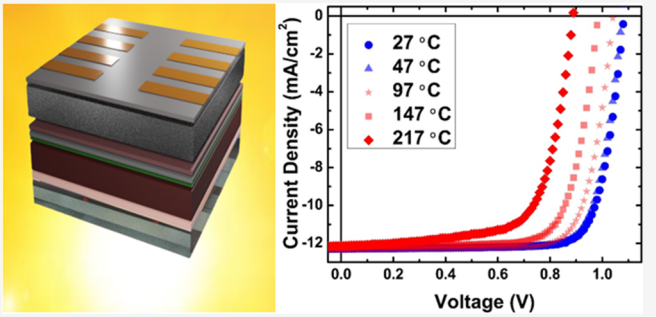

Metal halide perovskites have received considerable attention as a low-cost terrestrial photovoltaic (PV) technology. Perovskite PVs also display unique properties that may allow this technology to be commercially viable as a space PV technology, particularly their high radiation tolerance.[1,2] However, survival under space conditions requires more than just tolerance to radiation. One of the other high-risk areas for operation in space is the ability of a technology to withstand the high temperatures experienced in space—with satellites even in the Low Earth Orbits regularly experiencing temperatures as high as 120−140 °C (393−413 K).[3] Therefore, despite this tolerance to high-energy particle irradiation, questions remain with respect to the thermal stability of perovskite solar cells (PSCs). Several perovskite-specific phenomena such as ion motion, phase segregation, and/or outgassing of the constituent organic molecules raise questions with regard to thermal stability,[4] so there is a need to assess and stabilize their thermal response at high temperatures (>358 K, 85 °C) in the context of practical space applications[4,5] as well as to enable accelerated lifetime testing and stability assessment of perovskites for practical terrestrial applications, in general.

Triple halide and formamidinium cesium (FACs) based perovskite solar cells have been shown to be among the most stable perovskites to date.[6−9] While there have been a large number of studies on single gap PV applications, the triple halide systems have shown considerable promise—and are more appropriate—as the high energy junction in perovskite-perovskite,[10,11] silicon-perovskite,[12,13] and CIGS-perovskite[14,15] tandem solar cells. Earlier work has also demonstrated the high radiation tolerance of the metal halide perovskite systems for potential space power applications.[4,16,17] Here, high-temperature data are presented which systematically and statistically demonstrate the high thermal stability of this system at temperatures in excess of 200 °C.

In this study, the remarkable thermal operation of the FACs-triple halide perovskite solar cells is demonstrated. This is attributed to the specific design of the perovskite solar cells assessed, which were designed to survive severe high-temperature conditions using a cell architecture comprising three main components. First, a double cation (FACs) composition is used which has been shown to be among the most stable perovskite systems by the community. Second, a transparent conductive back contact was used to eliminate metal-induced degradation which may occur through metal migration or iodine−metal corrosion.[18] Finally, a conformal atomic layer deposition (ALD) of an alumina-based nanolaminate was deposited to prevent thermal decomposition via loss of volatile species. When combined, this creates a bifacial cell allowing independent assessment of transparent front and back surfaces optically, while correlating this to the PV performance of the solar cell at various radiation levels and temperatures between 250 and 490 K (−23 to 217 °C).

Received: March 14, 2023
Accepted: April 24, 2023
Published: April 27, 2023

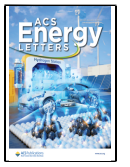

https://doi.org/10.1021/acsenergylett.3c00551
ACS Energy Lett. 2023, 8, 2408−2413

Figure 1a shows the schematic structure of the solar cell. The perovskite solar cells utilize a spin-coated

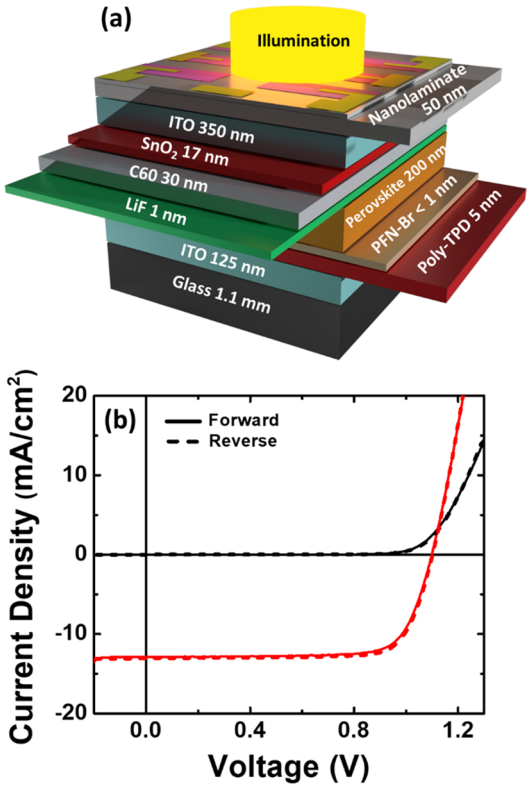

Figure 1. (a). Schematic of perovskite solar cell investigated in this study. Light is shown entering through the back Al_2O_3-based nanolaminate layer. (b) Representative dark (black) and light (red) $J-V$ curves at 1 sun AM1.5G.

$FA_{0.8}Cs_{0.2}Pb_{1.02}I_{2.4}Br_{0.6}Cl_{0.02}$ (~1.67 eV band gap, thickness = 200 nm) absorber layer integrated upon an indium tin oxide (ITO) back contact, a poly(*N*,*N*′-bis-4-butylphenyl-*N*,*N*′-bisphenyl)benzidine (Poly-TPD) hole transport layer, with a poly[(9,9-bis(3′-((*N*,*N*-dimethyl)-*N*-ethylammonium)-propyl)-2,7-fluorene)-*alt*-2,7-(9,9-dioctylfluorene)]dibromide (PFN-Br) interface layer to improve perovskite crystallization. The back of the cell architecture consists of a SnO_2/C_{60} electron transport layer separated from the back ITO contact by a thin LiF interfacial layer. A final 50 nm Al_2O_3-based nanolaminate layer encapsulates the device structure. Here, light is shown entering through the back (in Figure 1a) Al_2O_3-based encapsulant layer.

The absorber thickness here is lower than that of conventional perovskite solar cells to allow assessment of absorption. To assess the stability of the perovskite independently of any device stack degradation, the thermal stability of devices was also confirmed in devices with a more conventional 400 nm perovskite layer (see Figure SI 1 in the Supporting Information).

Initial assessments of the current density−voltage ($J-V$) responses of the devices were tested in the dark and under 1 sun AM1.5G illumination (see Figure 1b). The quality of these devices was confirmed via the lack of hysteresis and the high yield and reproducibility of a large series of (~100) solar cells comprising three generations of devices processed independently over 18 months (see Figure SI 2 in the Supporting Information).

Here, the focus is on measuring the $J-V$ characteristics for a series of devices from 250 K (−23 °C) up to 490 K (217 °C) in steps of 10 K under a vacuum of $\sim 10^{-3}$ Torr. At each temperature, both 1 sun AM1.5G and dark $J-V$ measurements were performed in both forward and reverse directions, with the devices held at each temperature for ~5 min. 300 K (approximately room temperature) is treated as the benchmark for the PV parameters. The study includes a 250−300 K range to show the typical behavior that has been previously reported: e.g., the steady increase of V_{oc} as a function of temperature that is due to the normal temperature dependence of the perovskite's band gap.[19,20] What is quite remarkable is the change in V_{oc} trend above 300 K from the normal low-temperature trend which is shown for the 250−300 K region.

The inset to Figure 2a shows temperature-dependent $J-V$ measurements taken using reverse voltage sweeps between 250

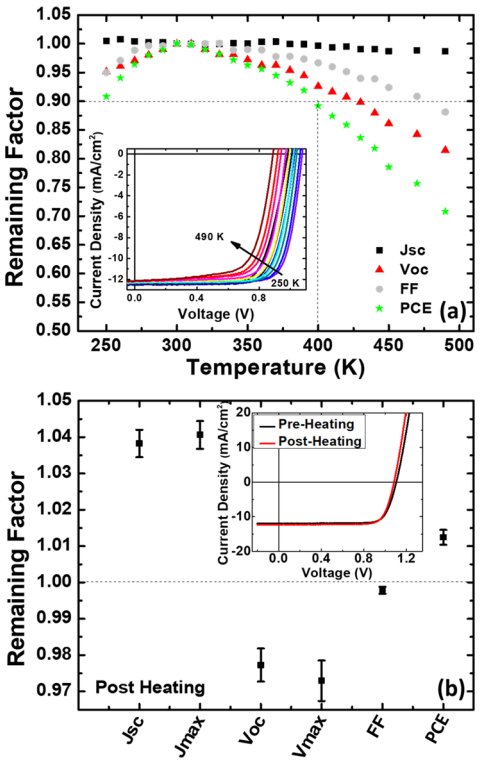

Figure 2. (a) The inset shows temperature-dependent $J-V$ results swept in the reverse direction from 300 K to 490 K. The main panel is a plot showing the temperature dependence of the remaining factors for PV parameters J_{sc}, V_{oc}, FF, and PCE extracted from the $J-V$ curves shown in the inset. (b) The inset shows the $J-V$ curve for 300 K under 1 sun AM1.5G measured before (black) and after (red) thermal cycle, demonstrating retention of performance despite the extreme thermal load under which they were exposed. The main panel is a plot of the remaining factors for room-temperature PV parameters post heating.

K (−23 °C) and 490 K (217 °C). When assessing both forward and reverse sweeps, evidence of hysteresis (Figure SI 3 in the Supporting Information) is observed above 400 K, indicating ion migration-halide segregation and appears as a loss of V_{oc}. Despite these high-temperature effects, the devices do not experience prohibitive degradation. Instead, upon returning to ambient temperatures they retain/reproduce their

https://doi.org/10.1021/acsenergylett.3c00551
ACS Energy Lett. 2023, 8, 2408−2413

original performance—in some cases there is a slight improvement after this high-temperature exposure.

The main panel of Figure 2a shows the temperature dependence for the remaining factor of key photovoltaic parameters extracted from the $J-V$ measurements shown in the inset to Figure 2a. The fill factor (FF: gray symbols Figure 2a) shows high tolerance to extremely high temperatures, retaining ~90% of its initial value at 490 K (217 °C). Typically, the FF of a perovskite solar cell is particularly sensitive to external perturbations, but here the stability of the FF indicates that the structural properties of the junction(s) and the device structure are not significantly affected by higher temperatures. Indeed, the absorber material and interfaces apparently remain intact at the high temperatures to which the devices are exposed. While V_{oc} (red triangles) is the PV parameter most affected by the increased temperature exposure above $T > 300$ K, it retains 80% of its initial value, and the combined effects of the PV parameters to high temperature is a loss of power conversion efficiency (PCE) that retains 70% of its initial ambient value at 490 K (217 °C).

On exposure to elevated temperatures, V_{oc} typically contributes to the reduction of solar cell efficiency as a result of the variations in the band gap and the consequential increase in the dark saturation current, as the band gap for conventional solar cells decreases.[21,22] However, since the band gap of perovskite systems increases—rather than decreases—with increasing temperature (as is illustrated by the temperature-dependent EQE in Figure 3a), the origin of the V_{oc} loss shown in Figure 2a at higher temperatures is subtler in perovskite solar cells than more traditional semiconductor solar cells such as silicon or the III–V systems. This is further supported by the constant J_{sc} (black squares) at elevated temperatures also shown in Figure 2a, which would also be perturbed if the dark current increased over this temperature range.

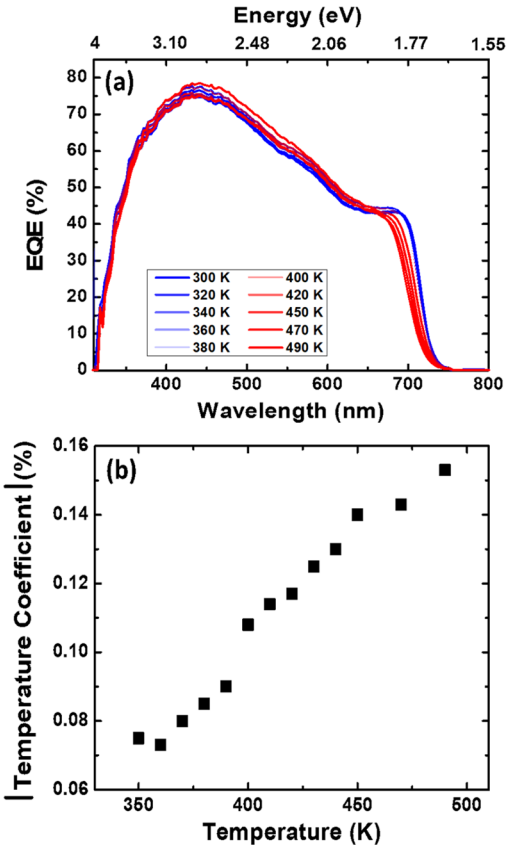

Figure 3. (a) Temperature-dependent external quantum efficiency between 300 K and 490 K showing an expected increase in the perovskite band gap. (b) Temperature dependence of the temperature coefficient between 350 K and 490 K.

Although this V_{oc} loss at higher temperatures requires further investigation, one possible explanation would be the onset of reversible halide segregation at higher temperatures under illumination. Such reversible halide segregation would result in iodine-rich regions in the absorber that have a reduced band gap, thus opening a pathway for lower V_{oc}. This is supported by the temperature dependence of the external quantum efficiency (EQE) described below (see Figure 3a), while the reversible nature of this process and the absence of prohibitive degradation of the solar cells studied after exposure to the high thermal stress are also supported by the absence of prohibitive degradation observed at 300 K at high excitation powers (up to 0.5 W, Figure SI-4 in the Supporting Information). Specifically, under high photoexcitation (~500 mW) reversible halide segregation is also observed as the lattice and carrier distribution heats with a local lattice temperature in excess of 450 K, returning to the original PL energy/linewidth at lower power.

This reversible behavior is also supported by the return to the original performance of the solar cells after this thermal cycle. The $J-V$ measurements at 1 sun AM1.5G at 300 K before and after the extreme high-temperature stress are shown as an inset to Figure 2b. The $J-V$ values retain much of their performance, and the devices appear relatively unaffected after high-temperature cycling, illustrating the reversible nature and lack of prohibitive degradation of the devices under such stress.

The main panel of Figure 2b depicts the remaining factor of the key PV parameters from the 1 sun AM1.5G $J-V$ measurements performed at 300 K *after* the solar cells were exposed to temperatures up to 490 K. These results reflect the data from multiple pixels on the device, and the error bars indicate the distribution in the results of all pixels/devices assessed.

As seen in Figure 2b, after undergoing the thermal stress not only do J_{sc} and J_{max} remain undegraded—they are apparently improved by 4%. It appears that not only is the stress received by the samples nondestructive or prohibitive to performance and stability, but also the thermal load provided to the devices appears to improve the performance presumably via "annealing" of the solar cells. This "annealing" serves to improve the quality of the interfaces and/or the transporting layers or absorber in the solar cell structure. The V_{oc} and V_{max} remaining factor values while degraded (Figure 2b), are by as little as 3% absolute, which can be attributed to the minor changes in the perovskite lattice due to annealing and the low crystallization temperature of these systems, or possibly to effects such as material homogenization and strain relaxation upon exposure to high temperature.[5]

The stability and resilience of the devices and the absence of degradation upon exposure are further supported by an assessment of the dark $J-V$ from the solar cells at 300 K (both before and after thermal cycling as shown in Figure SI-5 in the Supporting Information). These data show that not only does the dark J not increase after high-temperature exposure but also that the dark J experiences a reduction in the current level after high thermal stress. Moreover, these data did not

https://doi.org/10.1021/acsenergylett.3c00551
ACS Energy Lett. 2023, 8, 2408–2413

indicate significant increases in nonradiative processes at a higher temperature.

In these specific samples, it is possible that J_{sc} is relatively unaffected, since the thickness of the absorber layer is small, ~200 nm. This provides a sufficiently short path length for collection, compensating for reduced diffusion length that may be induced due to defects and decomposition at high temperatures. Such effects are also observed in ultrathin III–V solar cells under high-energy irradiation.[23]

However, it must be stressed once again that the stability and ability of these systems at $T \approx 490$ K is also observed in identical structures in which the thickness of the absorber was 400 nm as per conventional structures—see Figure SI-6 in the Supporting Information. As such, the stability presented cannot be attributed to the thinness of the absorber layer assessed here.

The unusual J_{sc} can also be understood in terms of the collection efficiency and band gap renormalization as a function of temperature. This can be further elucidated from the temperature-dependent EQE shown in Figure 3a. When extracting the J_{sc} values from the EQE data at room and high temperature a value of ~12 mA/cm^2 is determined, similar to the J_{sc} recorded in Figure 2a.

The high-temperature stability presented here is assessed under illumination only after the solar cells reach the temperature of assessment. Notably, thicker samples assessed under constant illumination (and held at V_{oc} or J_{sc} prior to J–V measurements—Figure SI-7 in the Supporting Information) during the temperature sweep also displayed remarkable tolerance to the thermal stress applied, further demonstrating the high stability of the double cation, triple halide systems under investigation here.

In previous high-temperature studies of perovskites it has been shown extensively[24−27] that there is some degradation/segregation and removal of the organic components (FA) around 473 K (200 °C). These studies have been mainly on films of the perovskite material (and not solar cells), since most previous perovskite solar cell technologies were not able to function consistently even at around 100 °C. Nevertheless, these high-temperature studies on the bulk perovskite materials (not solar cells) provided the PV community valuable information indicating that tailored perovskite systems may be capable of withstanding temperatures as high as 200 °C. Based on these works on high-T degradation mechanisms, one might expect severe decline of device performance above these temperatures, although having ultrathin (less than a micrometer) perovskite material layers sandwiched in tight structures changes the dynamics. Moreover, the time scales of FA degradation at high temperatures have been relatively unexplored.

Interestingly, Figure 2a indicates high-temperature tolerance for this perovskite composition (and the designed solar cell in total) specifically for J_{sc} that is relatively unaffected by this extreme temperature stress and remains relatively constant up to 490 K (217 °C). This is attributed to the thermal and structural stability of FACs-triple halide perovskites[28] and the effectiveness of the on-cell encapsulation used to package this system. Although the temperatures assessed here (up to 217 °C) exceed those in some other studies of perovskite solar cells (80 °C),[29] the robust nature of the performance observed is *not* unique to the perovskite studied. Rather, it is attributed to a combination of the absence of Spiro-OMeTAD, the implementation of ITO as the hole extraction contact, and the incorporation of an Al_2O_3-based encapsulation layer that appears to serve as a chemical barrier—presumably preventing the loss of even FA, which would be expected to be removed at such high temperatures.[21] Indeed, *less stable* $MAPbI_3$ thin films have been shown to withstand high temperatures (~150 °C) when encapsulated in glass and laminated to prevent the loss of constituent materials.[30]

The ability of encapsulation to increase the stabilization of perovskite devices, in general, has also recently been observed under high-fluence α and proton irradiation for devices encapsulated with a silicon oxide layer.[31] Those encapsulated devices demonstrated considerably higher stability than reference solar cells subjected to direct irradiation of the perovskite absorber without encapsulation. All of these studies indicate that when the constituent elements that comprise the perovskites are prevented from escaping, the dynamic nature of these systems facilitates self-healing and prevents prohibitive decomposition.[1]

When considering the EQE, the longer wavelengths display a reduced absolute EQE that reflects the thin absorber (nonoptimum thickness) used in this study. The high-temperature EQE (red curves) in Figure 3a has an absorption edge (therefore, band gap) at higher energy than the low-temperature EQE. This is as expected, considering the temperature dependence of the perovskite absorber. Importantly, the EQE spectra presented in Figure 3a indicate no evidence of a structural phase transition shift. Such effects serve to significantly and abruptly result in a red shift of the band gap (rather than the blue shift evident here). This is further support that the loss of performance or reduction in V_{oc} with increasing temperature is the result of halide segregation and ion migration. While the EQE measurements do not appear to indicate the presence of a structural phase transition, as the band edge does not show a sudden shift in energy, a structural phase transition cannot be totally excluded. These data also provide further evidence[19,20] of the stability of these systems as compared to single cation perovskite compounds. Hopefully these results will inspire further high-temperature elemental investigations of these less characterized perovskite compositions.

Interestingly, while the visible region of the EQE is almost unaffected at higher temperatures, the minor change occurs only at the expense of loss of longer wavelength absorption (tail of the EQE curve). This reflects the strong absorption due to excitons that dominate the optical properties of these systems, especially below ~200 K.[32−34] With an increase in temperature, the contribution of excitonic absorption subsequently reduces systematically as exciton ionization occurs; these states blue shift and merge into the continuum as the thermal energy (k_BT) increases. The transition from EQE dominated by excitonic complexes at low temperature to increased extraction at the shorter wavelengths at elevated temperatures results in an almost constant J_{sc} throughout this temperature range, as observed in Figure 2(a).

The unusual temperature dependence of the PV parameters in perovskite solar cells has led to temperature coefficients for maximum power (T_{PCE}) as low as −0.08% °C^{-1} which exceed those of typical commercial solar cell technologies such as silicon, CdTe, GaAs, and CIGS.[29] The temperature coefficient reflects the percentage of power lost by a solar cell as the temperature increases above the industry standard of 25 °C.[29] While the temperature coefficient is typically calculated with respect to room temperature since there is a larger reduction of

https://doi.org/10.1021/acsenergylett.3c00551
ACS Energy Lett. 2023, 8, 2408−2413

efficiency at higher temperatures, the upper limit of the temperature has a greater impact on the value of the temperature coefficient. Consequently, the higher the temperature, the larger the magnitude of the temperature coefficient.

Here, over a temperature range of 75−217 °C the temperature coefficient is determined to span −0.08 to −0.15% $°C^{-1}$. This compares favorably with previous analysis in perovskites and to that of other solar cell technologies[29] (see Table 1 in the Supporting Information) despite being evaluated at temperatures as high as 490 K (217 °C).

FACs triple halide perovskite solar cells with two thicknesses were exposed to extreme thermal stress ranging from −23 to 217 °C. The numerous solar cells assessed retained their performance when returning to ambient conditions after the very high temperature to which they were exposed, due to the choice of perovskite FACsPbIBrCl, transparent conductive back contact, and nanolaminite encapsulation. These devices *retained more than 90% of initial efficiency* at 400 K (127 °C), even with the onset of halide segregation at the highest temperatures assessed.

■ ASSOCIATED CONTENT

Supporting Information

The Supporting Information is available free of charge at https://pubs.acs.org/doi/10.1021/acsenergylett.3c00551.

> Experimental procedures (materials and device fabrication sections), photovoltaic characterization, temperature-dependent $J-V$ of a 400 nm thick solar cell from 300 K to 490 K, vomparison of the light $J-V$ results at room temperature for 3 different series of solar cells when they were received and several months later, forward and reverse sweeps of temperature-dependent $J-V$s from 300 K to 490 K, power-dependent photoluminescence at 295 K, dark $J-V$ measurements, temperature-dependent EQEs of a 400 nm thick solar cell for from 300 K to 450 K, temperature dependent $J-V$s held at J_{sc} and V_{oc} from 300 K to 490 K, and temperature coefficients (PDF)

■ AUTHOR INFORMATION

Corresponding Authors

Ian R. Sellers − *Department of Physics & Astronomy, University of Oklahoma, Norman, Oklahoma 73019, United States;* orcid.org/0000-0003-2782-0044; Email: sellers@ou.edu

Hadi Afshari − *Department of Physics & Astronomy, University of Oklahoma, Norman, Oklahoma 73019, United States;* orcid.org/0000-0001-7984-6313; Email: Hadi.Afshari-1@ou.edu

Authors

Shashi Sourabh − *Department of Physics & Astronomy, University of Oklahoma, Norman, Oklahoma 73019, United States*

Sergio A. Chacon − *Department of Physics & Astronomy, University of Oklahoma, Norman, Oklahoma 73019, United States*

Vincent R. Whiteside − *Department of Physics & Astronomy, University of Oklahoma, Norman, Oklahoma 73019, United States;* orcid.org/0000-0001-7846-3150

Rachel C. Penner − *Department of Physics & Astronomy, University of Oklahoma, Norman, Oklahoma 73019, United States*

Bibhudutta Rout − *Department of Physics, University of North Texas, Denton, Texas 76203, United States*

Ahmad R. Kirmani − *National Renewable Energy Laboratory, Golden, Colorado 80401, United States;* Present Address: Rochester Institute of Technology, Rochester, New York 14623, United States

Joseph M. Luther − *National Renewable Energy Laboratory, Golden, Colorado 80401, United States;* orcid.org/0000-0002-4054-8244

Giles E. Eperon − *Swift Solar, San Carlos, California 94070, United States*

Complete contact information is available at: https://pubs.acs.org/10.1021/acsenergylett.3c00551

Notes

The authors declare no competing financial interest.

■ ACKNOWLEDGMENTS

The authors are grateful for Axel Palmstrom's efforts in the ALD of the nanolaminate layer at NREL. This research was supported by the University of Oklahoma's Center for Quantum Research and Technology. UNT acknowledges partial support from NSF grant No. HBCU-EiR-2101181. This work was authored in part by the National Renewable Energy Laboratory, operated by the Alliance for Sustainable Energy, LLC, for the U.S. Department of Energy (DOE) under Contract No. DE-AC36-08GO28308. NREL authors were supported by the operational energy capability improvement fund (OECIF) of the Department of Defense. The views expressed in the article do not necessarily represent the views of the DOE or the U.S. Government.

■ REFERENCES

(1) Kirmani, A. R.; Durant, B. K.; Grandidier, J.; Haegel, N. M.; Kelzenberg, M. D.; Lao, Y. M.; McGehee, M. D.; McMillon-Brown, L.; Ostrowski, D. P.; Peshek, T. J.; et al. Countdown to perovskite space launch: Guidelines to performing relevant radiation-hardness experiments. *Joule* **2022**, *6*, 1015−1031.

(2) Ho-Baillie, A. W.; Sullivan, H. G.; Bannerman, T. A.; Talathi, H. P.; Bing, J.; Tang, S.; Xu, A.; Bhattacharyya, D.; Cairns, I. H.; McKenzie, D. R. Deployment opportunities for space photovoltaics and the prospects for perovskite solar cells. *Advanced Materials Technologies* **2022**, *7* (3), 2101059.

(3) Plante, J.; Lee, B. *Environmental conditions for space flight hardware: a survey*; NASA: 2005.

(4) Miyazawa, Y.; Ikegami, M.; Chen, H.-W.; Ohshima, T.; Imaizumi, M.; Hirose, K.; Miyasaka, T. Tolerance of Perovskite Solar Cell to High-Energy Particle Irradiations in Space Environment. *iScience* **2018**, *2*, 148−155.

(5) Mundt, L. E.; Zhang, F.; Palmstrom, A. F.; Xu, J.; Tirawat, R.; Kelly, L. L.; Stone, K. H.; Zhu, K.; Berry, J. J.; Toney, M. F.; et al. Mixing Matters: Nanoscale Heterogeneity and Stability in Metal Halide Perovskite Solar Cells. *ACS Energy Letters* **2022**, *7*, 471−480.

(6) Pavlovetc, I. M.; Brennan, M. C.; Draguta, S.; Ruth, A.; Moot, T.; Christians, J. A.; Aleshire, K.; Harvey, S. P.; Toso, S.; Nanayakkara, S. U.; et al. Suppressing cation migration in triple-cation lead halide perovskites. *ACS Energy Letters* **2020**, *5* (9), 2802−2810.

(7) Wu, X.; Jiang, Y.; Chen, C.; Guo, J.; Kong, X.; Feng, Y.; Wu, S.; Gao, X.; Lu, X.; Wang, Q.; et al. Stable triple cation perovskite precursor for highly efficient perovskite solar cells enabled by

interaction with 18C6 stabilizer. *Adv. Funct. Mater.* **2020**, *30* (6), 1908613.
(8) Xu, J.; Boyd, C. C.; Yu, Z. J.; Palmstrom, A. F.; Witter, D. J.; Larson, B. W.; France, R. M.; Werner, J.; Harvey, S. P.; Wolf, E. J.; et al. Triple-halide wide-band gap perovskites with suppressed phase segregation for efficient tandems. *Science* **2020**, *367* (6482), 1097−1104.
(9) Xu, K.; Al-Ashouri, A.; Peng, Z.-W.; Kohnen, E.; Hempel, H.; Akhundova, F.; Marquez, J. A.; Tockhorn, P.; Shargaieva, O.; Ruske, F.; et al. Slot-Die Coated Triple-Halide Perovskites for Efficient and Scalable Perovskite/Silicon Tandem Solar Cells. *ACS Energy Letters* **2022**, *7* (10), 3600−3611.
(10) Lin, R.; Xu, J.; Wei, M.; Wang, Y.; Qin, Z.; Liu, Z.; Wu, J.; Xiao, K.; Chen, B.; Park, S. M.; et al. All-perovskite tandem solar cells with improved grain surface passivation. *Nature* **2022**, *603* (7899), 73−78.
(11) Heo, J. H.; Im, S. H. CH3 NH3 PbBr3 -CH3 NH3 PbI3 Perovskite-Perovskite Tandem Solar Cells with Exceeding 2.2 V Open Circuit Voltage. *Advanced materials (Deerfield Beach, Fla.)* **2016**, *28* (25), 5121−5.
(12) Liu, J.; De Bastiani, M.; Aydin, E.; Harrison, G. T.; Gao, Y.; Pradhan, R. R.; Eswaran, M. K.; Mandal, M.; Yan, W.; Seitkhan, A.; Babics, M.; Subbiah, A. S.; Ugur, E.; Xu, F.; Xu, L.; Wang, M.; Rehman, A. u.; Razzaq, A.; Kang, J.; Azmi, R.; Said, A. A.; Isikgor, F. H.; Allen, T. G.; Andrienko, D.; Schwingenschlögl, U.; Laquai, F.; De Wolf, S. Efficient and stable perovskite-silicon tandem solar cells through contact displacement by MgFx. *Science* **2022**, *377* (6603), 302−306.
(13) Al-Ashouri, A.; Köhnen, E.; Li, B.; Magomedov, A.; Hempel, H.; Caprioglio, P.; Márquez, J. A.; Morales Vilches, A. B.; Kasparavicius, E.; Smith, J. A.; Phung, N.; Menzel, D.; Grischek, M.; Kegelmann, L.; Skroblin, D.; Gollwitzer, C.; Malinauskas, T.; Jošt, M.; Matič, G.; Rech, B.; Schlatmann, R.; Topič, M.; Korte, L.; Abate, A.; Stannowski, B.; Neher, D.; Stolterfoht, M.; Unold, T.; Getautis, V.; Albrecht, S. Monolithic perovskite/silicon tandem solar cell with > 29% efficiency by enhanced hole extraction. *Science* **2020**, *370* (6522), 1300−1309.
(14) Jošt, M.; Köhnen, E.; Al-Ashouri, A.; Bertram, T.; Tomšič, S.; Magomedov, A.; Kasparavicius, E.; Kodalle, T.; Lipovšek, B.; Getautis, V.; Schlatmann, R.; Kaufmann, C. A.; Albrecht, S.; Topič, M. Perovskite/CIGS Tandem Solar Cells: From Certified 24.2% toward 30% and Beyond. *ACS Energy Letters* **2022**, *7* (4), 1298−1307.
(15) Han, Q.; Hsieh, Y.-T.; Meng, L.; Wu, J.-L.; Sun, P.; Yao, E.-P.; Chang, S.-Y.; Bae, S.-H.; Kato, T.; Bermudez, V.; Yang, Y. High-performance perovskite/Cu(In,Ga)Se2 monolithic tandem solar cells. *Science* **2018**, *361* (6405), 904−908.
(16) Durant, B. K.; Afshari, H.; Singh, S.; Rout, B.; Eperon, G. E.; Sellers, I. R. Tolerance of Perovskite Solar Cells to Targeted Proton Irradiation and Electronic Ionization Induced Healing. *ACS Energy Lett.* **2021**, *6*, 2362−2368.
(17) Tu, Y.; Wu, J.; Xu, G.; Yang, X.; Cai, R.; Gong, Q.; Zhu, R.; Huang, W. Perovskite Solar Cells for Space Applications: Progress and Challenges. *Adv. Mater.* **2021**, *33* (21), 2006545.
(18) Besleaga, C.; Abramiuc, L. E.; Stancu, V.; Tomulescu, A. G.; Sima, M.; Trinca, L.; Plugaru, N.; Pintilie, L.; Nemnes, G. A.; Iliescu, M.; et al. Iodine migration and degradation of perovskite solar cells enhanced by metallic electrodes. *journal of physical chemistry letters* **2016**, *7* (24), 5168−5175.
(19) Brown, C. R.; Eperon, G. E.; Whiteside, V. R.; Sellers, I. R. Potential of High-Stability Perovskite Solar Cells for Low-Intensity-Low-Temperature (LILT) Outer Planetary Space Missions. *ACS Appl. Energy Mater.* **2019**, *2* (1), 814−821.
(20) Afshari, H.; Durant, B. K.; Kirmani, A. R.; Chacon, S. A.; Mahoney, J.; Whiteside, V. R.; Scheidt, R. A.; Beard, M. C.; Luther, J. M.; Sellers, I. R. Temperature-Dependent Carrier Extraction and the Effects of Excitons on Emission and Photovoltaic Performance in Cs0. 05FA0. 79MA0. 16Pb (I0. 83Br0. 17) 3 Solar Cells. *ACS Appl. Mater. Interfaces* **2022**, *14* (39), 44358−44366.
(21) Singh, P.; Ravindra, N. M. Temperature dependence of solar cell performance-an analysis. *Sol. Energy Mater. Sol. Cells* **2012**, *101*, 36−45.
(22) Al-Khazzar, A. A. A. Behavior of four Solar PV modules with temperature variation. *Int. J. Renew. Energy Res.* **2016**, *6* (3), 1091−1099.
(23) Hirst, L.; Yakes, M.; Warner, J.; Bennett, M.; Schmieder, K.; Walters, R.; Jenkins, P. Intrinsic radiation tolerance of ultra-thin GaAs solar cells. *Appl. Phys. Lett.* **2016**, *109* (3), 033908.
(24) Ma, L.; Guo, D.; Li, M.; Wang, C.; Zhou, Z.; Zhao, X.; Zhang, F.; Ao, Z.; Nie, Z. Temperature-Dependent Thermal Decomposition Pathway of Organic-Inorganic Halide Perovskite Materials. *Chem. Mater.* **2019**, *31* (20), 8515−8522.
(25) Kundu, S.; Kelly, T. L. In situ studies of the degradation mechanisms of perovskite solar cells. *EcoMat* **2020**, *2* (2), No. e12025.
(26) Nagabhushana, G.; Shivaramaiah, R.; Navrotsky, A. Direct calorimetric verification of thermodynamic instability of lead halide hybrid perovskites. *Proc. Natl. Acad. Sci. U. S. A.* **2016**, *113* (28), 7717−7721.
(27) Zhou, J.; Zhang, J.; Chen, S.; Zhao, F.; Qiu, L.; Meng, Z.; Ding, L.; Wang, B.; Pan, Q. Comparative Thermal Research on Energetic Molecular Perovskite Structures. *Molecules* **2022**, *27* (3), 805.
(28) Donakowski, A.; Miller, D. W.; Anderson, N. C.; Ruth, A.; Sanehira, E. M.; Berry, J. J.; Irwin, M. D.; Rockett, A.; Steirer, K. X. Improving photostability of cesium-doped formamidinium lead triiodide perovskite. *ACS Energy Letters* **2021**, *6* (2), 574−580.
(29) Moot, T.; Patel, J. B.; McAndrews, G.; Wolf, E. J.; Morales, D.; Gould, I. E.; Rosales, B. A.; Boyd, C. C.; Wheeler, L. M.; Parilla, P. A.; Johnston, S. W.; Schelhas, L. T.; McGehee, M. D.; Luther, J. M. Temperature Coefficients of Perovskite Photovoltaics for Energy Yield Calculations. *ACS Energy Lett.* **2021**, *6*, 2038−2047.
(30) Dunfield, S. P.; Moore, D. T.; Klein, T. R.; Fabian, D. M.; Christians, J. A.; Dixon, A. G.; Dou, B.; Ardo, S.; Beard, M. C.; Shaheen, S. E.; et al. Curtailing perovskite processing limitations via lamination at the perovskite/perovskite interface. *ACS Energy Letters* **2018**, *3* (5), 1192−1197.
(31) Kirmani, A. R.; Ostrowski, D. P.; VanSant, K. T.; Byers, T. A.; Bramante, R. C.; Heinselman, K. N.; Tong, J.; Stevens, B.; Nemeth, W.; Zhu, K.; Sellers, I. R.; Rout, B.; Luther, J. M. Metal oxide barrier layers for terrestrial and space perovskite photovoltaics. *Nature Energy* **2023**, *8*, 191−202.
(32) Marongiu, D.; Saba, M.; Quochi, F.; Mura, A.; Bongiovanni, G. The role of excitons in 3D and 2D lead halide perovskites. *J. Mater. Chem. C* **2019**, *7* (39), 12006−12018.
(33) Baranowski, M.; Urban, J.; Zhang, N.; Surrente, A.; Maude, D.; Andaji-Garmaroudi, Z.; Stranks, S.; Plochocka, P. Static and dynamic disorder in triple-cation hybrid perovskites. *J. Phys. Chem. C* **2018**, *122* (30), 17473−17480.
(34) Baranowski, M.; Plochocka, P. Excitons in metal-halide perovskites. *Adv. Energy Mater.* **2020**, *10* (26), 1903659.

https://doi.org/10.1021/acsenergylett.3c00551
ACS Energy Lett. 2023, 8, 2408−2413